Article:
Townrow, Oliver P.E., Weller, Andrew S. orcid.org/0000-0003-1646-8081 and Goicoechea, Jose M. (2024) Controlled cluster expansion at a Zintl cluster surface. Angewandte Chemie International Edition. e202316120. ISSN 1433-7851

https://doi.org/10.1002/anie.202316120

A Journal of the Gesellschaft Deutscher Chemiker

Angewandte International Edition GDCh Chemie

www.angewandte.org

Accepted Article

Title: Controlled Cluster Expansion at a Zintl Cluster Surface

Authors: Oliver Townrow, Andrew Weller, and Jose Goicoechea

To be cited as: *Angew. Chem. Int. Ed.* **2023**, e202316120

Link to VoR: https://doi.org/10.1002/anie.202316120

WILEY VCH

10.1002/anie.202316120

WILEY VCH

RESEARCH ARTICLE

Controlled cluster expansion at a Zintl cluster surface

Oliver P. E. Townrow,[a] Andrew S. Weller,*[b] and Jose M. Goicoechea*[c]

[a] Dr. O. P. E. Townrow
Department of Chemistry
University of Oxford
Chemistry Research Laboratory, 12 Mansfield Road, Oxford, OX1 3TA, U.K.

[b] Prof. Dr. A. S. Weller
Department of Chemistry
University of York
Heslington, York, YO10 5DD, U.K.
E-mail: andrew.weller@york.ac.uk

[c] Prof. Dr. J. M. Goicoechea
Department of Chemistry
Indiana University
800 E. Kirkwood Ave., Bloomington, IN., 47405, U.S.A.
E-mail: jgoicoec@iu.edu

Supporting information for this article is given via a link at the end of the document.

Abstract: Reaction of the tris-hypersilyl nonagermanide Zintl cluster salt, $K[Ge_9(Hyp)_3]$ (Hyp = $Si(SiMe_3)_3$) with $[Rh(\eta^2,\eta^2\text{-L})Cl]_2$ (L = 1,5-cyclooctadiene, COD; norbornadiene, NBD) afforded eleven- and twelve-vertex *homo*-multimetallic clusters by cluster core expansion. Using a stepwise procedure, starting from the Zintl cluster $[Rh(COD)\{Ge_9(Hyp)_3\}]$ and $[Ir(COD)Cl]_2$, this methodology was expanded for the synthesis of eleven-vertex *hetero*-multimetallic clusters. A mechanism for the formation of these first examples of *closo* eleven-vertex Zintl clusters is proposed, informed by density functional theory calculations.

Introduction

Transition metal main group element alloys (TMMGAs) integrate the highly reactive properties of the late transition metals with the low melting points of the heavier main group elements. At elevated temperatures these molten alloys contain “solvated” catalytically active transition metal atoms in a main group element matrix.[1] These alloys have been used as catalysts for industrially relevant processes such as the dehydrogenation of light alkanes to produce dihydrogen and alkenes, or graphitic carbon on complete dehydrogenation.[1–5]

Crucially, the ratio of the elements employed in such alloys appears to have a significant influence on the catalytic efficacy of TMMGAs. For example, Wasserscheid and co-workers recently demonstrated that for rhodium/gallium liquid mixtures, varying the rhodium:gallium ratio from 1:125 (where single atoms of rhodium are present in the melt), to 1:25 (where intermetallic compounds are formed at the alloy surface), resulted in a significant change in productivity for the catalytic dehydrogenation of propane, with the former showing the highest performance over the entirety of the temperature range sampled.[6]

These studies prompted us to investigate Zintl clusters containing transition metals and main group (semi-)metals as hydrocarbon soluble molecular models for TMMGAs. Such species have previously been postulated as model single atom catalysts.[7] This led to the synthesis of the first Zintl cluster found to be active in homogeneous catalysis: $[Rh(COD)\{Ge_9(Hyp)_3\}]$ (**A;** COD = 1,5-cyclooctadiene).[8] More recently, we extended these studies to show that related clusters are competent catalysts for H/D exchange and C−H bond activation processes.[9] Our work shows that Zintl clusters have the potential to be optimized to give precisely defined molecular species that mimic the impressive reactivity of TMMGAs. To best achieve this goal, it would be useful to be able to tailor the transition metal to main group element ratio, in order to complement the compositional diversity available when using alloys. In this work, we present the controlled modification of rhodium:germanium ratios in Zintl clusters through a cluster core expansion strategy. We also show that it is possible to use this stepwise strategy to access hetero-multimetallic compounds containing rhodium, iridium and germanium. While reactions of substituent-free Zintl clusters $[E_9]^{4-}$ (E = Si–Pb) with transition metal reagents are known to give rise to multi-metallic species in which cluster fragmentation often takes place,[10] here we show that the nuclearity of nonagermanide clusters can be sequentially built up by addition of one, two and three transition metal fragments to access ten-, eleven- and twelve-vertex clusters in a controlled fashion.

Results and Discussion

$K[Ge_9(Hyp)_3]$ was initially reacted with one equivalent of $[Rh(COD)Cl]_2$ (i.e. Rh:Ge = 2:9) at –78 °C in toluene solution. The reaction vessel was allowed to gradually warm to room temperature yielding a mixture of products from which **A**,[8] and the novel bimetallic cluster $[\{Rh(COD)\}_2\{Ge_9(Hyp)_3Cl\}]$ (**1**) were isolated in low yields (<10 %). This reaction is accompanied by extensive decomposition which we believe arises from the low solubility of $K[Ge_9(Hyp)_3]$ at these temperatures, and the resultant non-stoichiometric ratio of reactants in solution. To avoid such undesirable low yields, the bimetallic compound **1** can instead be selectively prepared (>85% isolated yield) using a stepwise synthesis starting from preformed **A** (Scheme 1).[8] These reactions indicate that stepwise cluster assembly is desirable over

10.1002/anie.202316120

WILEY VCH

RESEARCH ARTICLE

a simple one-pot reaction, where the rhodium precursor and $K[Ge_9(Hyp)_3]$ are combined in the appropriate ratio.

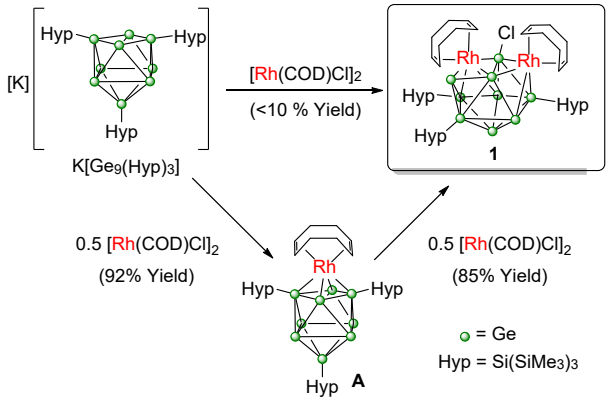

Scheme 1. Synthetic pathways to [{Rh(COD)}$_2${Ge_9(Hyp)$_3$Cl}] (**1**).

The ^{1}H NMR (nuclear magnetic resonance) spectrum of **1** shows the loss of resonances corresponding to the hypersilyl substituents of the precursor (0.29 and 0.57 ppm) and the appearance of new resonances at 0.50, 0.54 and 0.69 ppm (in a 1:1:1 ratio). This indicates the generation of a low symmetry complex that is not fluxional on the NMR timescale. In addition to this, multiple new resonances between 1.4 and 5.7 ppm are observed, the integrals of which are consistent with two magnetically inequivalent COD ligands. The ^{29}Si/^{1}H HMBC (Heteronuclear Multiple Bond Correlation) NMR spectrum exhibits four ^{29}Si signals at –79.74, –74.85, –62.92 and –8.16 ppm and six cross peaks (suggesting that two of the ^{29}Si NMR signals arise from 1+1 overlapping resonances). This further confirms the presence of three inequivalent hypersilyl substituents (see Supporting Information).

Red-brown crystals of **1** suitable for single-crystal X-ray diffraction were obtained from an *n*-hexane solution stored at −40 °C.[11] The asymmetric unit contains one molecule of compound **1** and half a molecule of *n*-hexane. As can be seen in the crystal structure of the product (Figure 1), the reaction resulted in the addition of a Rh(COD) fragment to **A**, forming an eleven-atom cage from the ten-atom cluster precursor. This is in contrast to the reaction of compound **1** with $[Ni(COD)_2]$, which under similar conditions yielded the trimetallic cluster [Rh(COD){Ni(COD)}$_2${Ge_9(Hyp)$_3$}], where the Ni(COD) fragments coordinate in an η^3 'capping' fashion to the sides of the bicapped square antiprismatic cluster rather than being incorporated into the cluster core.[8]

In addition to the increase in nuclearity, a chloride substituent, originating from the $[Rh(COD)Cl]_2$ precursor, is retained in the product, having been transferred to an adjacent germanium atom (Ge6). The hypersilyl substituents have also rearranged (as supported by DFT calculations; *vide infra*), two of which are now attached to adjacent germanium atoms. To the best of our knowledge this is the first example of a Zintl cluster possessing an *exo*-halide bond.

The cluster core in **1** adopts an asymmetric, edge-contracted icosahedral geometry containing two Rh(COD) vertices bridged by two germanium vertices. One Rh(COD) fragment is coordinated in an η^4 mode to the germanium support (Rh1 as labelled in Figure 1), as in **A**.[8] The second Rh(COD) vertex (Rh2) sits in an η^5-coordination site of the cage, as observed in [Rh(DPPE){η^5-Ge_9(Hyp)$_3$}] (DPPE = bis(diphenylphosphino)-ethane),[8] and the $[M(CO)_3\{\eta^5\text{-}Ge_9(Hyp)_3\}]^-$ (M = Cr, Mo, W) series reported by Schnepf.[12,13] Compound **1** is a *closo* eleven-vertex deltahedron with 24 valence electrons available for cluster bonding (Rh(COD) = 2 × 1 e$^-$, Ge = 5 × 2 e$^-$, Ge(Hyp) = 3 × 3 e$^-$, Ge(Cl) = 1 × 3 e$^-$). It is isostructural and valence isoelectronic to the only two structurally characterized edge-contracted icosahedral clusters $[B_{11}H_{11}]^{2-}$ and $[B_{11}H_{10}(SMe_2)]^-$.[14,15] Zintl clusters with eleven vertices are uncommon and none of the examples reported to date have a *closo* electron count.[16] The synthesis of **1** represents a rare instance of a *closo* to *closo* cluster expansion reaction.[17] Similar transformations are known in the chemistry of carboranes, although they tend to proceed *via* reduced *nido* species that are generated *in situ*.[18,19]

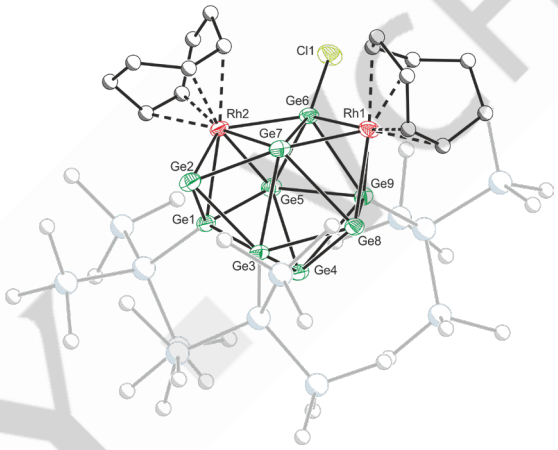

Figure 1. Single crystal X-ray structure of compound **1**. Anisotropic displacement ellipsoids set at 50% probability. All carbon and silicon atoms are pictured as spheres of arbitrary radii. Hydrogen atoms and solvent of crystallization are omitted for clarity. Selected bond lengths (Å): Rh1–Ge6: 2.380(1), Rh1–Ge7: 2.535(1), Rh1–Ge8: 2.592(1), Rh1–Ge9: 2.687(1), Rh2–Ge1: 2.514(1), Rh2–Ge2: 2.614(1), Rh2–Ge5: 2.861(1), Rh2–Ge6: 2.415(1), Rh2–Ge7: 2.681(1), Ge6–Cl1 2.251(1), Ge1–Si1 2.456(2), Ge3–Si5 2.418(2), Ge9–Si9 2.420(2).

Interested in extending the stepwise methodology used for the synthesis of **1**, we attempted to access heterobimetallic complexes with a complementary topology. We proposed that using a different metal reagent would also allow us to determine which of the rhodium metal centers present in **1** was originally present in the precursor, **A**, and thus allow us to understand the mechanism of cluster growth. The second metal should thus ideally contribute the same number of electrons and have a similar steric profile to Rh(COD) to retain the *closo* 24 valence electron count. For this purpose, $[Ir(COD)Cl]_2$ was used as the precursor in the synthesis of a Rh/Ir heterobimetallic complex, [{Rh(COD)}{Ir(COD)}{Ge_9(Hyp)$_3$Cl}] (**2**) (Scheme 2).

A toluene solution of compound **A** cooled to –78 °C was added to a toluene suspension of $[Ir(COD)Cl]_2$ at the same temperature, then stirred for 3 hours at ambient temperature. The resulting brown solution was dried *in vacuo* and extracted into *n*-pentane to remove a small amount of black solid. The solvent was removed *in vacuo* and the resultant brown solid lyophilized from benzene. It was found that performing the reaction and workup in the dark improved yields and decreased the formation of black insoluble decomposition products. Compound **2** is moderately

10.1002/anie.202316120

RESEARCH ARTICLE

unstable in solution and decomposes completely within three days at room temperature to an intractable mixture, indicated by broadening and subsequent loss of the ^{1}H NMR resonances relating to the hypersilyl substituents, which limited the study of further reactivity.

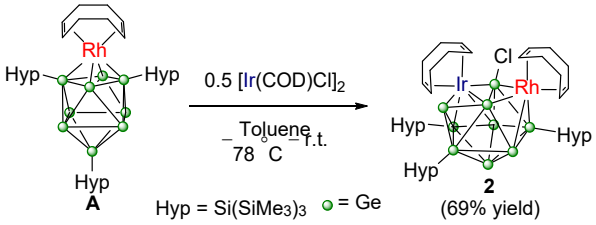

Scheme 2. Preparation of [{Rh(COD)}{Ir(COD)}{Ge$_9$(Hyp)$_3$Cl}] (**2**).

The NMR spectra of compound **2** are qualitatively similar to that of **1**, indicating, again, a loss of C_{2v} symmetry (see Supporting Information). Dark red crystals of compound **2** suitable for single-crystal X-ray diffraction were obtained from an *n*-hexane solution stored at −40 °C. The molecular structure (Figure 2) exhibits the same cluster topology as compound **1** with the two transition metal centers occupying unique sites, confirming incorporation of an Ir(COD) vertex. There is no evidence of positional disorder at the sites occupied by the two metal centers.

At the η^4 coordinated Rh(COD) vertex, all bond lengths are similar to compound **1**, differing by no more than ±0.01 Å in either the Rh–Ge or Rh–C distances. The η^5 coordinated Ir(COD) vertex is also similar to its rhodium counterpart in compound **1**, accounting for the slight increase in radius (~0.02 Å).[20,21]

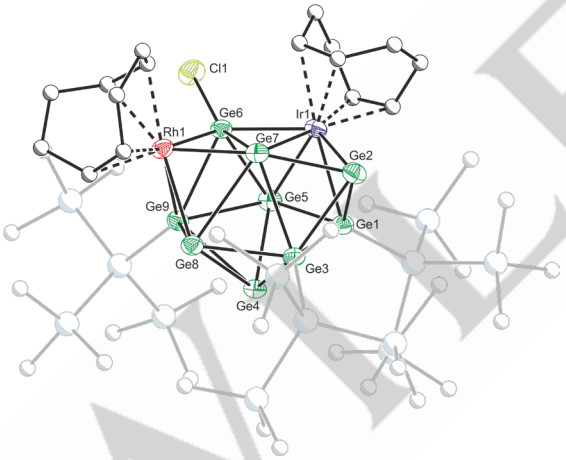

Figure 2. Single crystal X-ray structure of compound **2**. Anisotropic displacement ellipsoids set at 50% probability. All carbon and silicon atoms are pictured as spheres of arbitrary radius. Hydrogen atoms are omitted for clarity. Selected bond lengths (Å): Selected bond lengths (Å): Rh1–Ge6: 2.375(1), Rh1–Ge7: 2.541(1), Rh1–Ge8: 2.588(1), Rh1–Ge9: 2.691(1), Ir1–Ge1: 2.519(1), Ir1–Ge2: 2.606(1), Ir1–Ge5: 2.861(1), Ir1–Ge6: 2.424(1), Ir1–Ge7: 2.700(1), Ge6–Cl1 2.244(2), Ge1–Si1 2.458(2), Ge3–Si5 2.417(2), Ge9–Si9 2.412(2).

Since the Ir(COD) fragment is valence isoelectronic to Rh(COD), compound **2** has the same electronic structure as compound **1** and can also be classified as an eleven-vertex *closo* deltahedron with 24 valence electrons available for cluster bonding. Given the similar covalent and ionic size of rhodium(I) and iridium(I), previous reports of η^4 bound Ir(COD) fragments on tetrel Zintl clusters,[17,22] and the absence of scrambling between metal fragments over the η^4 and η^5 sites, we can deduce that the Rh(COD) group at the η^4 vertex (Rh1) in both **1** and **2** most likely originates from the precursor compound **A**.

To investigate this further, density functional theory at the BP86-D3/Def2-TZVP (polarizable continuum model = benzene) level of theory was employed to elucidate a thermochemically feasible mechanism starting from **A** and half an equivalent of [Rh(COD)Cl]$_2$ (see Supporting Information, Figure S10, for full details and alternative considered pathways). The computed reaction pathway reveals four key processes. The first step involves *exo*-coordination of a Rh(COD)Cl fragment to the electron rich *closo*-cage (–18.8 kJ mol^{-1}), which is followed by chloride transfer from rhodium to a germanium vertex (–8.3 kJ mol^{-1}). This process has a barrier of 30.9 kJ mol^{-1}. From there, rhodium insertion into the cluster core affords an eleven-vertex cluster with an η^5-coordinated rhodium center. This is an exergonic step (–20.1 kJ mol^{-1}) with a low activation barrier of 27.6 kJ mol^{-1}. Finally, hypersilyl transfer from one germanium vertex to an adjacent, less sterically hindered, germanium center requires an activation energy of 67.8 kJ mol^{-1} to afford the product, which is (overall) –85.8 kJ mol^{-1} lower in energy that the reagents. Evidence for this type of migration has been postulated by Sevov for the fluxional processes present in the tetra-functionalized cluster [Ge$_9$(Hyp)$_3$Et].[23,24] Alternative cluster formation pathways were ruled out due to higher activation barriers.

Isolation of compound **1** prompted us to ask whether a second *closo* to *closo* cluster expansion may allow access to a twelve-vertex trimetallic icosahedron, a geometry that is ubiquitous in cluster chemistry.[25] However, adding further equivalents of [Rh(COD)Cl]$_2$ to **1** resulted in no observable change by ^{1}H NMR spectroscopy. We reasoned that this may be due to the bulky COD ligands sterically restricting further reactivity and therefore turned to the use of [Rh(NBD)Cl]$_2$ (NBD = norbornadiene), which contains a smaller diene, as the rhodium precursor.

The stepwise methodology used for the preparation of compound **1** led us to first target [Rh(NBD){Ge$_9$(Hyp)$_3$}], the NBD-containing analogue of **A**, by adding 0.5 equivalents of [Rh(NBD)Cl]$_2$ to K[Ge$_9$(Hyp)$_3$]. Analysis of the reaction mixture by ^{1}H NMR spectroscopy, however, did not display the expected two hypersilyl resonances in a 2:1 ratio between 0 and 1 ppm. Instead, unreacted K[Ge$_9$(Hyp)$_3$] was observed, in addition to three peaks in a 1:1:1 ratio relating to three inequivalent hypersilyl NMR resonances that signaled a loss of symmetry. Addition of [Rh(NBD)Cl]$_2$ (1 eq.) to this mixture consumed the excess K[Ge$_9$(Hyp)$_3$], and increased the intensities of the resonances associated with the new species. In addition, nine broad signals relating to NBD ligands were observed.

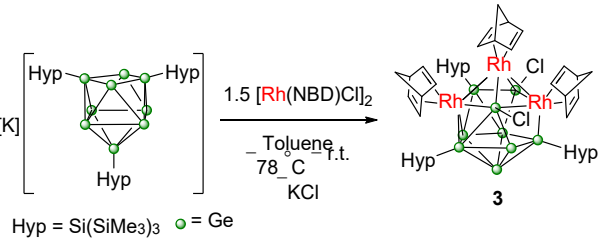

Scheme 3. Preparation of [{Rh(NBD)}$_3${Ge$_9$(Hyp)$_3$Cl$_2$}] (**3**).

The experiment was repeated with one and a half equivalents of [Rh(NBD)Cl]$_2$ in toluene solution at –78 °C and allowed to warm

10.1002/anie.202316120

to room temperature overnight (Scheme 3). Crystallization from *n*-pentane at –80 °C produced dark red crystals of [{Rh(NBD)}$_3${Ge$_9$(Hyp)$_3$Cl$_2$}] (**3**) in an 80% isolated yield.

The asymmetric unit of compound **3** contains one crystallographically unique molecule of **3** and 1.5 equivalents of *n*-pentane as solvent of crystallization (Figure 3). The cluster has a distorted *closo* 12-vertex icosahedral geometry and can be interpreted as a *closo* twelve-vertex deltahedron with 26 valence electrons available for cluster bonding (Rh(NBD) = 1 × 1 e$^-$, Ge = 5 × 2 e$^-$, Ge(Hyp) = 3 × 3 e$^-$, Ge(Cl) = 1 × 3 e$^-$).

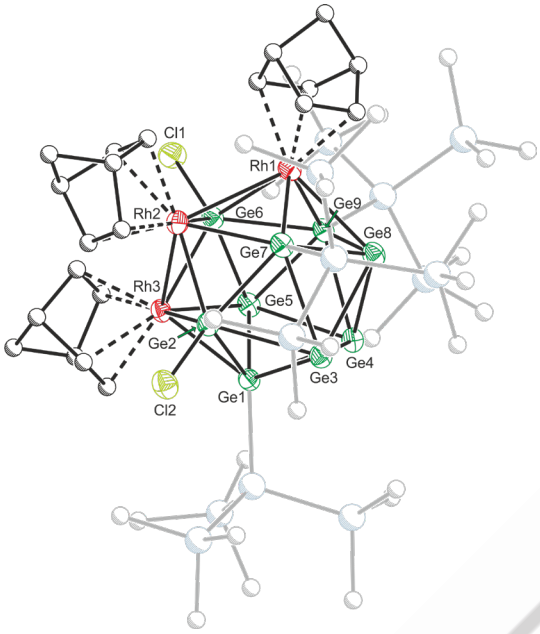

Figure 3. Single crystal X-ray structure of compound **3**. Anisotropic displacement ellipsoids set at 50% probability. All carbon and silicon atoms are pictured as spheres of an arbitrary radius. Hydrogen atoms are omitted for clarity. Selected bond lengths (Å): Rh1–Ge6: 2.470(1), Rh1–Ge7: 2.482(1), Rh1–Ge8: 2.723(1), Rh1–Ge9: 2.606(1), Rh1–Rh2: 2.989(1), Rh2–Ge2: 2.415(1), Rh2–Ge6: 2.499(1), Rh2–Ge7: 2.551(1), Rh2–Rh3: 3.119(1), Rh3–Ge1: 2.541(1), Rh3–Ge2: 2.489(1), Rh3–Ge5: 2.682(1), Rh3–Ge6: 2.418(1), Ge2–Cl2: 2.210(1), Ge6–Cl1: 2.243(1), Ge1–Si1: 2.428(1), Ge7–Si5: 2.457(1), Ge9–Si9: 2.419(1).

The structure shows two Rh(NBD) fragments (Rh1 and Rh3) coordinated in an η^5 mode by four germanium atoms and a central rhodium atom, with Rh–Ge distances in the range of 2.4148(4) to 2.5510(4) Å. The central Rh2 binds in an η^5 coordination mode, bonding to three germanium atoms and the two flanking rhodium atoms with Rh–Ge distances in the range of 2.4177(3) to 2.7229(4) Å. The rhodium vertices are separated by 2.9892(2) and 3.1194(3) Å, which are longer than predicted for a discrete single bond.[20] Two chlorine atoms (Cl1 and Cl2) have been transferred to adjacent germanium (Ge3 and Ge9) atoms, similar to compounds **1** and **2**.

The Rh–C distances range between 2.170(5) and 2.206(3) Å and are, on average, slightly shorter for the central Rh(NBD) than the flanking Rh(NBD) environments. These bond lengths are comparable to [Rh(NBD)(L)] complexes in the literature, for example: [Rh(NBD)(Ind)] (2.07(1) to 2.15(1) Å) (Ind = indenyl),[26] [Rh(NBD)(Tol)][SbF_6] (2.09(2) to 2.13(1) Å),[27] and [Rh(NBD)(DPPE)][BF_4] (2.207(3) to 2.236(3) Å).[28]

Conclusion

In conclusion, this work describes the controlled expansion of [Rh(η^2,η^2-L){Ge$_9$(Hyp)$_3$}] (L = diene) clusters by reactions at the cluster core, showing that the Zintl cluster support itself can take part in further reactivity. By reacting K[Ge$_9$(Hyp)$_3$] or **A** with group 9 metal alkene complexes, we were able to prepare a series of novel homo- and hetero-polymetallic clusters which retain their diene ligands, advantageous for potential applications in catalysis. This demonstrates some unique capabilities of a Zintl cluster based complex over traditional transition metal compounds featuring organic ligands as molecular models for TMMGAs.

Supporting Information

The authors have cited additional references within the Supporting Information.[29–44]

Acknowledgements

We thank Shell Global Solutions International B.V., the University of Oxford and the EPSRC for financial support of this research (Industrial CASE studentship O.P.E.T.; EP/M024210 ASW). The University of Oxford is also acknowledged for access to Chemical Crystallography facilities.

Keywords: Zintl clusters • metal alloys • germanium • rhodium • iridium

[1] D. C. Upham, V. Agarwal, A. Khechfe, Z. R. Snodgrass, M. J. Gordon, H. Metiu, E. W. McFarland, *Science* **2017**, *358*, 917–921.

[2] N. Taccardi, M. Grabau, J. Debuschewitz, M. Distaso, M. Brandl, R. Hock, F. Maier, C. Papp, J. Erhard, C. Neiss, W. Peukert, A. Görling, H.-P. Steinrück, P. Wasserscheid, *Nat. Chem.* **2017**, *9*, 862–867.

[3] C. Palmer, M. Tarazkar, H. H. Kristoffersen, J. Gelinas, M. J. Gordon, E. W. McFarland, H. Metiu, *ACS Catal.* **2019**, *9*, 8337–8345.

[4] C. Palmer, D. C. Upham, S. Smart, M. J. Gordon, H. Metiu, E. W. McFarland, *Nat. Catal.* **2020**, *3*, 83–89.

[5] T. Daeneke, K. Khoshmanesh, N. Mahmood, I. A. De Castro, D. Esrafilzadeh, S. J. Barrow, M. D. Dickey, K. Kalantar-Zadeh, *Chem. Soc. Rev.* **2018**, *47*, 4073–4111.

[6] N. Raman, S. Maisel, M. Grabau, N. Taccardi, J. Debuschewitz, M. Wolf, H. Wittkämper, T. Bauer, M. Wu, M. Haumann, C. Papp, A. Görling, E. Spiecker, J. Libuda, H.-P. Steinrück, P. Wasserscheid, *ACS Catal.* **2019**, *9*, 9499–9507.

[7] M. Neumaier, C. Schenk, H. Schnöckel, A. Schnepf, *Z. Anorg. Allg. Chem.* **2014**, *640*, 2701–2707.

[8] O. P. E. Townrow, C. Chung, S. A. Macgregor, A. S. Weller, J. M. Goicoechea, *J. Am. Chem. Soc.* **2020**, *142*, 18330–18335.

[9] O. P. E. Townrow, S. B. Duckett, A. S. Weller, J. M. Goicoechea, *Chem. Sci.* **2022**, *13*, 7626–7633.

[10] For recent reviews see: a) K. Mayer, J. Weßing, T. F. Fässler, R. A. Fischer, *Angew. Chem. Int. Ed.* **2018**, *57*, 14372–14393; b) B. Weinert,

S. Mitzinger, S. Dehnen, *Chem. Eur. J.* **2018**, *24*, 8470–8490; c) C. Liu, Z. M. Sun, *Coord. Chem. Rev.* **2019**, *382*, 32–56; d) Y. Wang, J. E. McGrady, Z. M. Sun, *Acc. Chem. Res.* **2021**, *54*, 1506–1516; e) F. Pan, B. Weinert, S. Dehnen, *Struct. Bond.* **2021**, *188*, 103–148; f) J.-X. Zhang, F. K. Sheong, Z. Lin, *Struct. Bond.* **2021** *188*, 197–258; g) J. E. McGrady, F. Weigand, S. Dehnen, *Chem. Soc. Rev.* **2022**, *51*, 628–649.

[11] Deposition numbers 2299684 (for **1**·0.5hex), 2299685 (for **2**·0.5hex), and 2299686 (for **3**·1.5pent) contain the supplementary crystallographic data for this paper. These data are provided free of charge by the joint Cambridge Crystallographic Data Centre and Fachinformationszentrum Karlsruhe Access Structures service.

[12] C. Schenk, A. Schnepf, *Chem. Commun.* **2009**, *22*, 3208–3210.

[13] F. Henke, C. Schenk, A. Schnepf, *Dalton Trans.* **2011**, *40*, 6704–6710.

[14] E. H. Wong, L. Prasad, E. J. Gabe, M. G. Gatter, *Inorg. Chem.* **1983**, *22*, 1143–1146.

[15] O. Volkov, W. Dirk, U. Englert, P. Paetzold, *Z. Anorg. Allg. Chem.* **1999**, *625*, 1193–1200.

[16] C. C. Shu, H. W. T. Morgan, L. Qiao, J. E. McGrady, Z. M. Sun, *Nat. Commun.* **2020**, *11*, 3477.

[17] J.-Q. Wang, S. Stegmaier, B. Wahl, T. F. Fässler, *Chem. Eur. J.* **2010**, *16*, 1793–1798.

[18] L. Qiao, J. E. McGrady, Z. M. Sun, *Zintl Chemistry: From Zintl ions to Zintl clusters, Chapter 14, Comprehensive Inorganic Chemistry III.* in Reference Module in Chemistry, Molecular Sciences and Chemical Engineering, Elsevier, Amsterdam 2021.

[19] F. Zheng, T. H. Yui, J. Zhang, Z. Xie, *Nat. Commun.* **2020**, *11*, 5943.

[20] P. Pyykkö, *J. Phys. Chem. A* **2014**, *119*, 2326–2337.

[21] R. D. Shannon, *Acta Crystallogr. Sect. A* **1976**, *32*, 751–767.

[22] D. O. Downing, P. Zavalij, B. W. Eichhorn, *Eur. J. Inorg. Chem.* **2010**, *2010*, 890–894.

[23] F. Li, S. C. Sevov, *J. Am. Chem. Soc.* **2014**, *136*, 12056–12063.

[24] F. Li, A. Muñoz-Castro, S. C. Sevov, *Angew. Chem. Int. Ed.* **2016**, *55*, 8630–8633.

[25] T. Fässler, G. S. Armatas, *Zintl Ions: Principles and Recent Developments*; Structure and Bonding, Springer-Verlag Berlin Heidelberg, Heidelberg, 2011.

[26] C. Bonifaci, A. Ceccon, A. Gambaro, P. Ganis, S. Santi, G. Valle, A. Venzo, *Organometallics* **1993**, *12*, 4211–4214.

[27] U. Kölle, R. Görissen, T. Wagner, *Chem. Ber.* **1995**, *128*, 911–917.

[28] H. J. Drexler, S. Zhang, A. Sun, A. Spannenberg, A. Arrieta, A. Preetz, D. Heller, *Tetrahedron Asymmetry* **2004**, *15*, 2139–2150.

[29] F. Li, S. C. Sevov, *Inorg. Chem.* **2012**, *51*, 2706–2708.

[30] G. Giordano, R. H. Crabtree, *Inorg. Synth.* **1979**, *19*, 218–219

[31] A. B. Chaplin, J. F. Hooper, A. S. Weller, M. C. Willis, *J. Am. Chem. Soc.* **2012**, *134*, 4885–4897.

[32] J. Cosier, A. M. Glazer, *J. Appl. Crystallogr.* **1986**, *19*, 105−107.

[33] *CrysAlisPro*, Agilent Technologies, Version 1.171.39.46e (Rigaku OD, 2018).

[34] a) G. M. Sheldrick in SHELXL97, *Programs for Crystal Structure Analysis* (Release 97-2), Institut für Anorganische Chemie der Universität, Tammanstrasse 4, D-3400 Göttingen, Germany, 1998; b) G. M. Sheldrick, *Acta Crystallogr. Sect. A* **1990**, *46*, 467−473; c) G. M. Sheldrick, *Acta Crystallogr. Sect. A* **2008**, *64*, 112−122. d) C. B. Hubschle, G. M. Sheldrick, B. Dittrich, *J. Appl. Crystallogr.* **2011**, *44*, 1281−1284.

[35] Gaussian 16, Revision A.03, M. J. Frisch, G. W. Trucks, H. B. Schlegel, G. E. Scuseria, M. A. Robb, J. R. Cheeseman, G. Scalmani, V. Barone, G. A. Petersson, H. Nakatsuji, X. Li, M. Caricato, A. V. Marenich, J. Bloino, B. G. Janesko, R. Gomperts, B. Mennucci, H. P. Hratchian, J. V. Ortiz, A. F. Izmaylov, J. L. Sonnenberg, D. Williams-Young, F. Ding, F. Lipparini, F. Egidi, J. Goings, B. Peng, A. Petrone, T. Henderson, D. Ranasinghe, V. G. Zakrzewski, J. Gao, N. Rega, G. Zheng, W. Liang, M. Hada, M. Ehara, K. Toyota, R. Fukuda, J. Hasegawa, M. Ishida, T. Nakajima, Y. Honda, O. Kitao, H. Nakai, T. Vreven, K. Throssell, J. A. Montgomery, Jr., J. E. Peralta, F. Ogliaro, M. J. Bearpark, J. J. Heyd, E. N. Brothers, K. N. Kudin, V. N. Staroverov, T. A. Keith, R. Kobayashi, J. Normand, K. Raghavachari, A. P. Rendell, J. C. Burant, S. S. Iyengar, J. Tomasi, M. Cossi, J. M. Millam, M. Klene, C. Adamo, R. Cammi, J. W. Ochterski, R. L. Martin, K. Morokuma, O. Farkas, J. B. Foresman and D. J. Fox, Gaussian Inc., Wallingford CT, 2016.

[36] A. D. Becke, *Phys. Rev. A* **1998**, *38*, 3098.

[37] J. P. Perdew, *Phys. Rev. B* **1986**, *33*, 8822.

[38] D. Andrae, U. Häußermann, M. Dolg, H. Stoll, H. Preuß, *Theor. Chim. Acta.* **1990**, *77*, 123–141.

[39] W. Ehlers, M. Böhme, S. Dapprich, A. Gobbi, A. Höllwarth, V. Jonas, K. F. Köhler, R. Stegmann, A.Veldkamp, G. Frenking, *Chem. Phys. Lett.* **1993**, *208*, 111–114.

[40] A. Höllwarth, M. Böhme, S. Dapprich, A. W. Ehlers, A. Gobbi, V. Jonas, K. F. Köhler, R. Stegmann, A. Veldkamp, G. Frenking, *Chem. Phys. Lett.* **1993**, *208*, 237–240.

[41] W. J. Hehre, R. Ditchfield, J. A. Pople, *J. Chem. Phys.* **1972**, *56*, 2257–2261.

[42] P. C. Hariharan, J. A. Pople, *Theor. Chim. Acta.* **1973**, *28*, 213–222.

[43] F. Weigend, R. Ahlrichs *Phys. Chem. Chem. Phys.* **2005**, *7*, 3297–3305.

[44] S. Grimme, J. Antony, S. Ehrlich, H. Krieg, *J. Chem. Phys.* **2010**, *132*, 154104.

10.1002/anie.202316120

WILEY VCH

RESEARCH ARTICLE

Entry for the Table of Contents

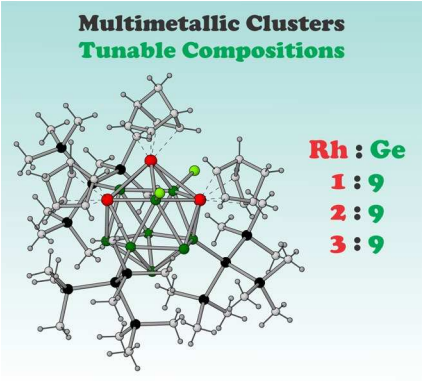

The stepwise growth of eleven- and twelve-vertex multimetallic clusters from a ten-atom precursor is demonstrated. These rare examples of closo- to closo- cluster expansion reactions offer insight into the mechanisms by which Zintl clusters assemble in solution. The resultant clusters possess exo-bonds to chlorine atoms that may allow for post-synthetic functionalization and their incorporation into materials.

Institute and/or researcher Twitter usernames: @GoicoecheaGroup, @WellerYorkChem, @olie_chem